Supplementary Information

Conformation Driven Conductance Modulation in Single-Stranded RNA (ssRNA)

Arpan De[1,#], Arindam K Das[2] and M. P. Anantram[1]

[1]Department of Electrical and Computer Engineering, University of Washington, Seattle, WA 98195, USA
[2]Department of Computer Science and Electrical Engineering, Eastern Washington University, Cheney, WA, 99004, USA

[#]Corresponding author: arpan99@uw.edu

Contents:

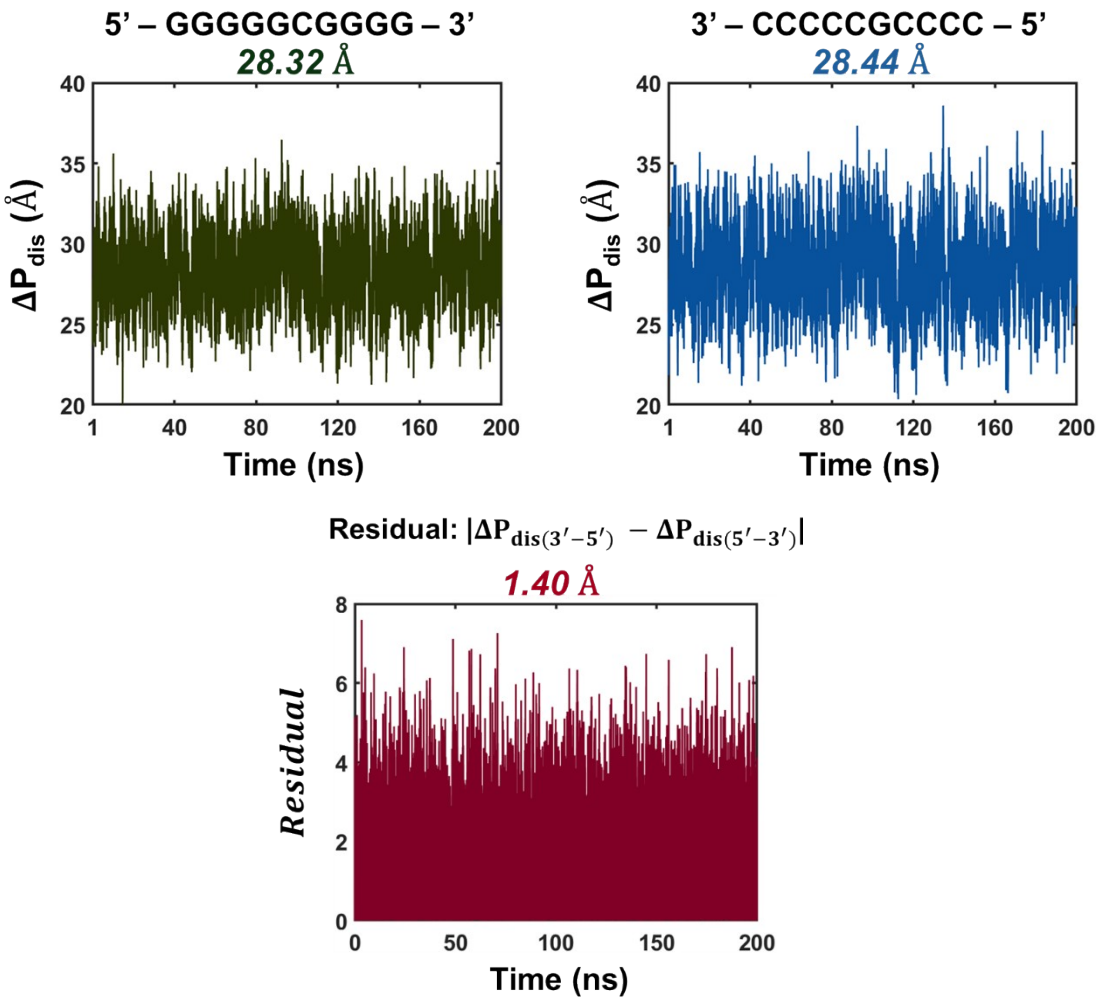

Figure S1: (Top row) Comparison of end-to-end phosphorus distances ($^{\Delta P_{dis}}$) in dsRNA between (Left) 5'-3' and (Right) 3'-5' strands. While the average $^{\Delta P_{dis}}$ in the 5'-3' strand is 28.32 Å, and in the 3'-5' strand is 28.44 Å. This shows that variations of $^{\Delta P_{dis}}$ in both strands are similar. (Bottom row) The difference between $^{\Delta P_{dis}}$ of the two strands in a dsRNA. The mean values are noted at the top of each figure.

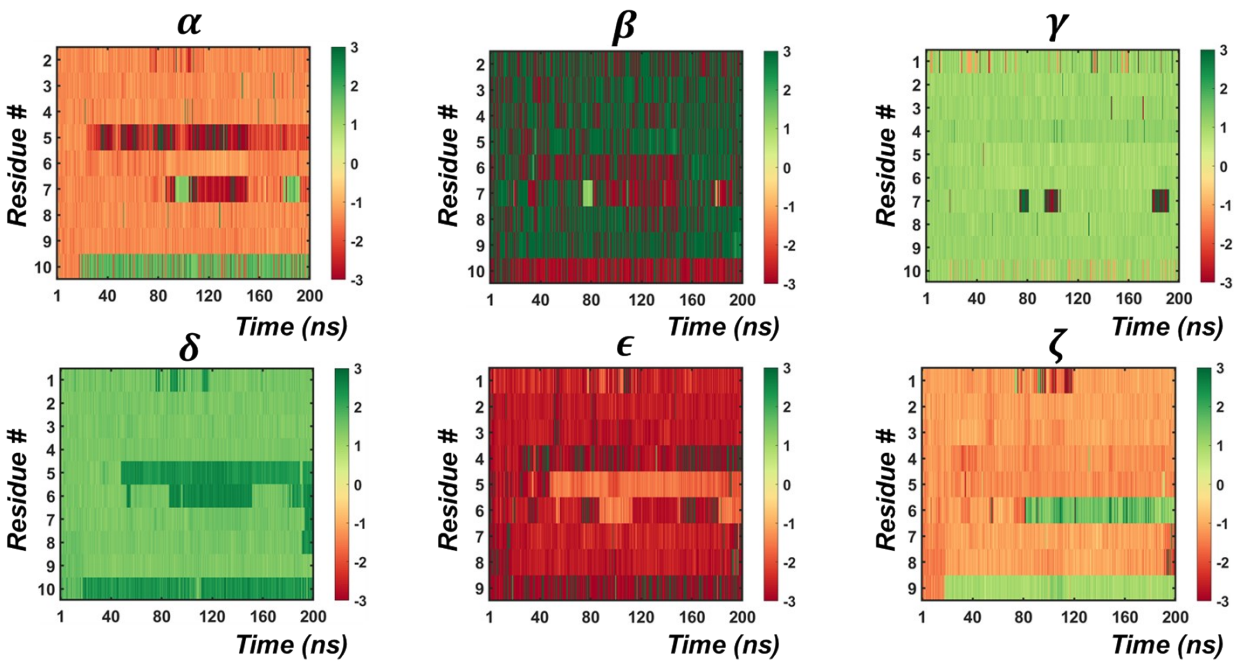

Figure S2: Time evolution of backbone dihedral angles in ssRNA. The corresponding angles are mentioned at the top of each heatmap. For every plot, the dihedral angle of each residue is shown as a function of time. The color bar has units of radians. In dsRNA, the values of γ and δ are always positive, while α, ϵ, and ζ are always negative (Figure S3). The fluctuations in the dihedral angles of ssRNA are large, and these values take both positive and negative values as a result of fluctuations.

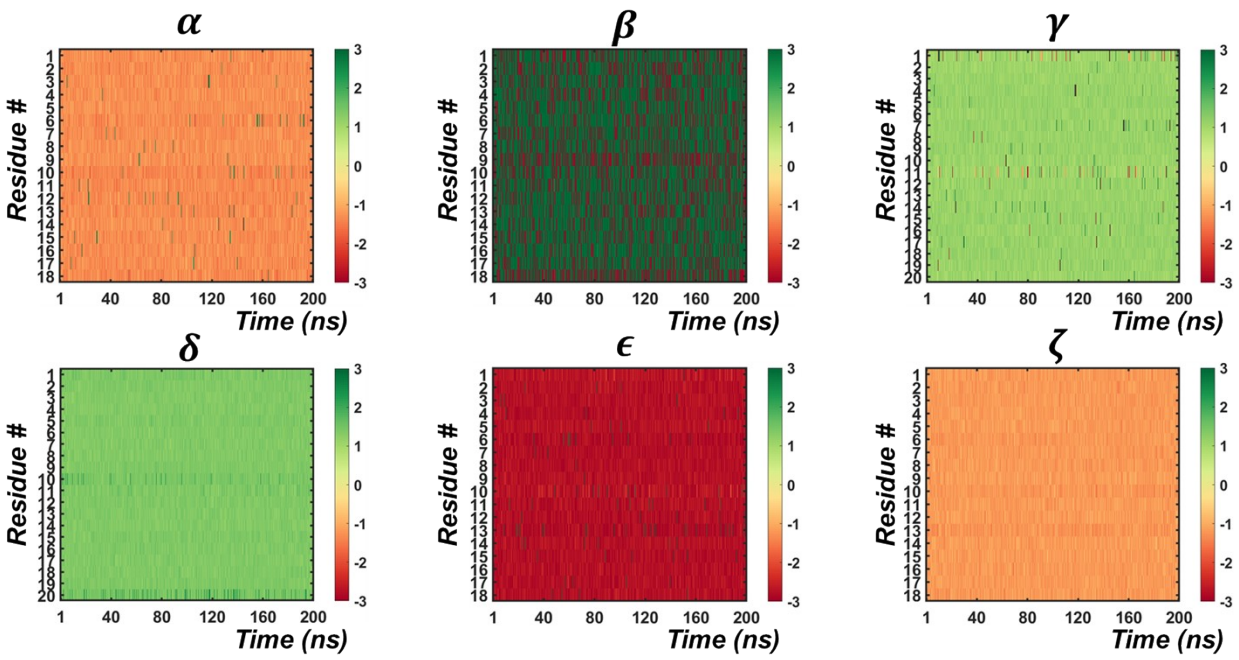

Figure S3: Time evolution of backbone dihedral angles in dsRNA. The corresponding angles are mentioned at the top of each heatmap. For every plot, the dihedral angle of each residue is shown as a function of time. The color bar has units of radians. The values of γ and δ are always positive, while α, ϵ, and ζ are always negative. In comparison to the backbone dihedral angles of the ssRNA (Figure S2), their dihedral angles do not change significantly with time.

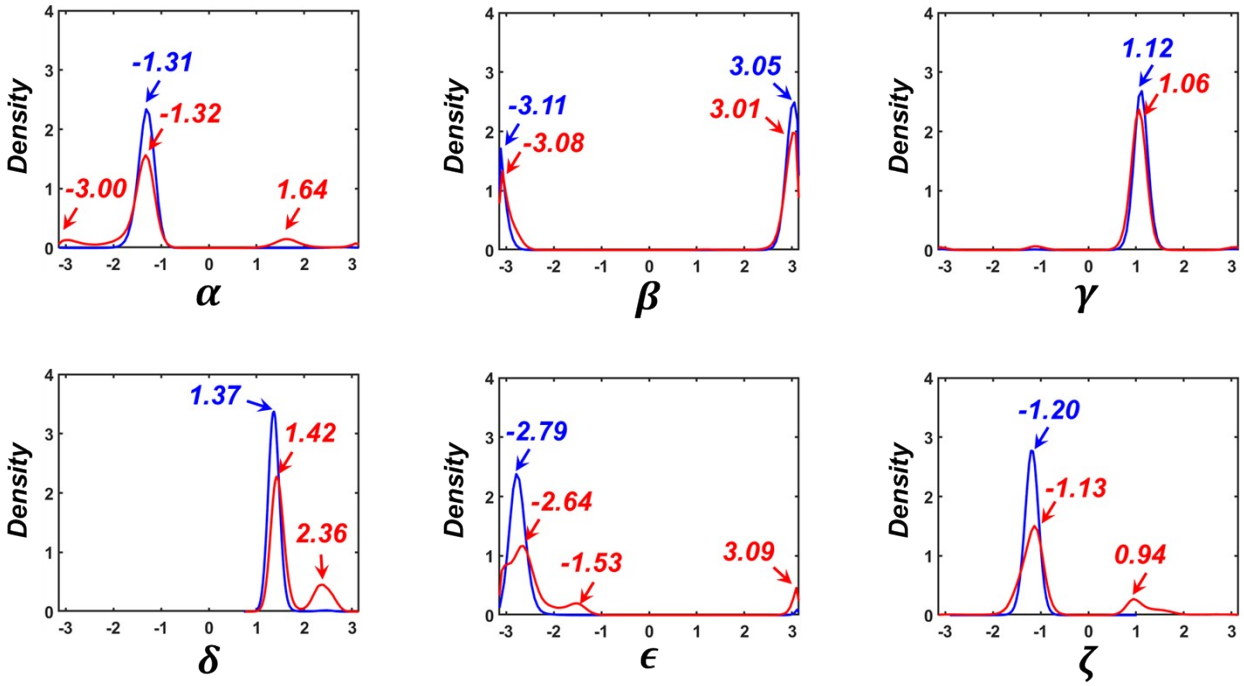

Figure S4: Kernel density estimates (KDE) of ssRNA (in red) and dsRNA (in blue) for the six backbone dihedral angles (in radians). The peaks are marked with arrows, and the numbers indicate the peak locations. Structural fluctuations of ssRNA induce a multimodal nature of the density estimates, which is indicative of lower stability. We have considered equal weight for each conformation during *density* estimation.

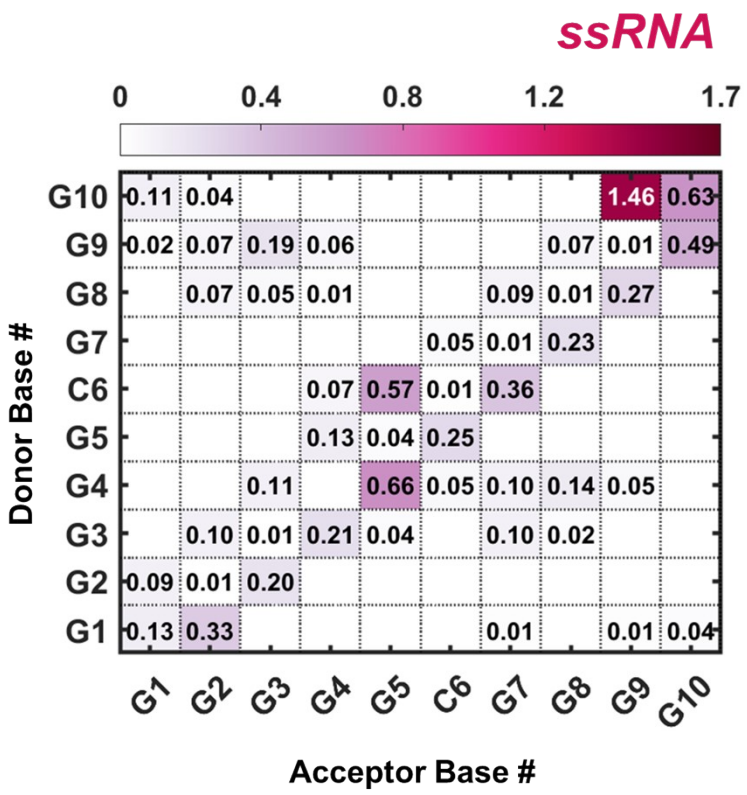

Figure S5-(i): Hydrogen heatmaps for ssRNA with average hydrogen bonds between different bases over 200 ns. The large off-diagonal numbers show hydrogen bonding between non-adjacent bases in comparison to dsRNA shown in Figure S5(ii).

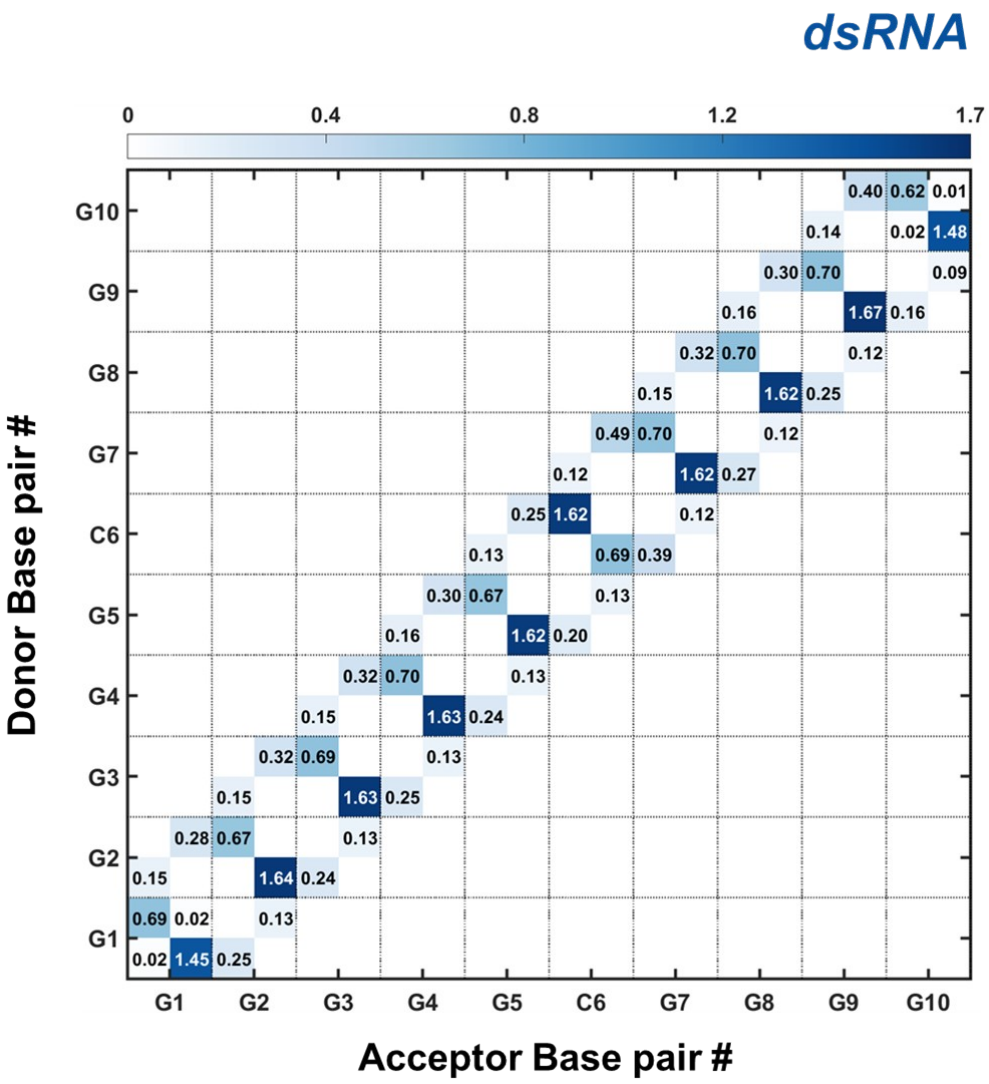

Figure S5-(ii): Hydrogen heatmaps for dsRNA with average hydrogen bonds between different base pairs over 200 ns.

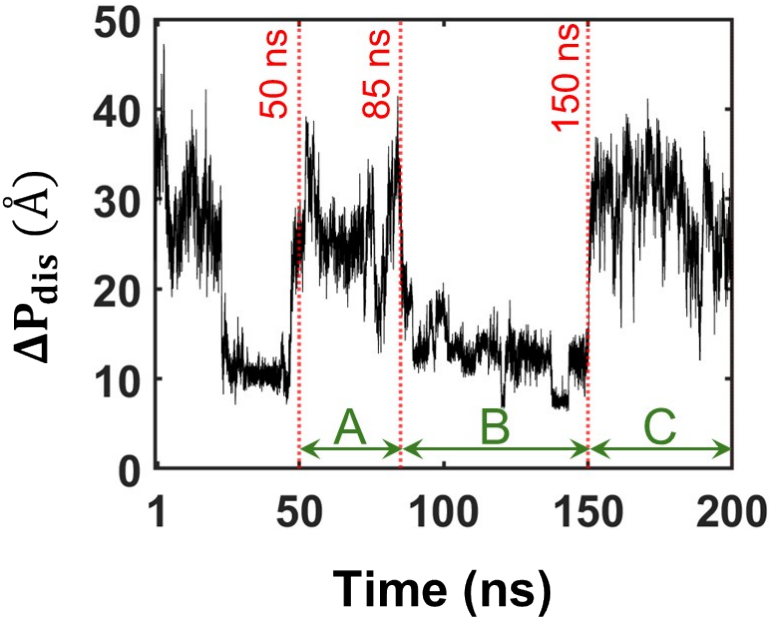

Figure S6-(i): Classification of different regions during MD trajectory to highlight folded and unfolded domains. The selected windows to demonstrate H-bond heatmaps in folded vs unfolded regimes are (A: 50-85 ns), (B: 85-150 ns), and (C: 150-200 ns), where overall $^{\Delta P_{dis}}$ is high, low, and high respectively.

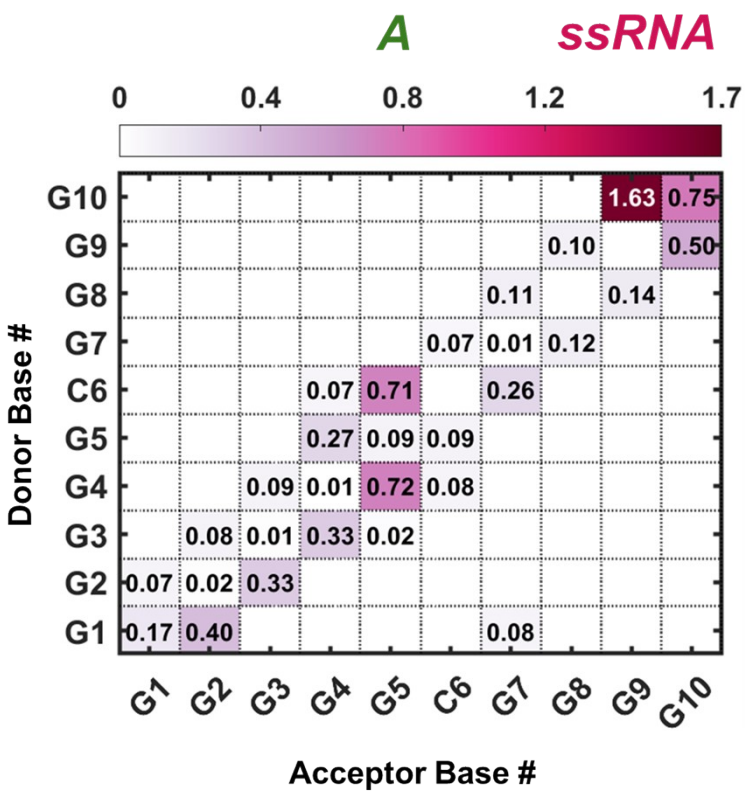

Figure S6-(ii): Hydrogen-bond (H-bond) heatmaps in time window – A, ranging from 50 to 85 ns, where overall ΔP_{dis} is high.

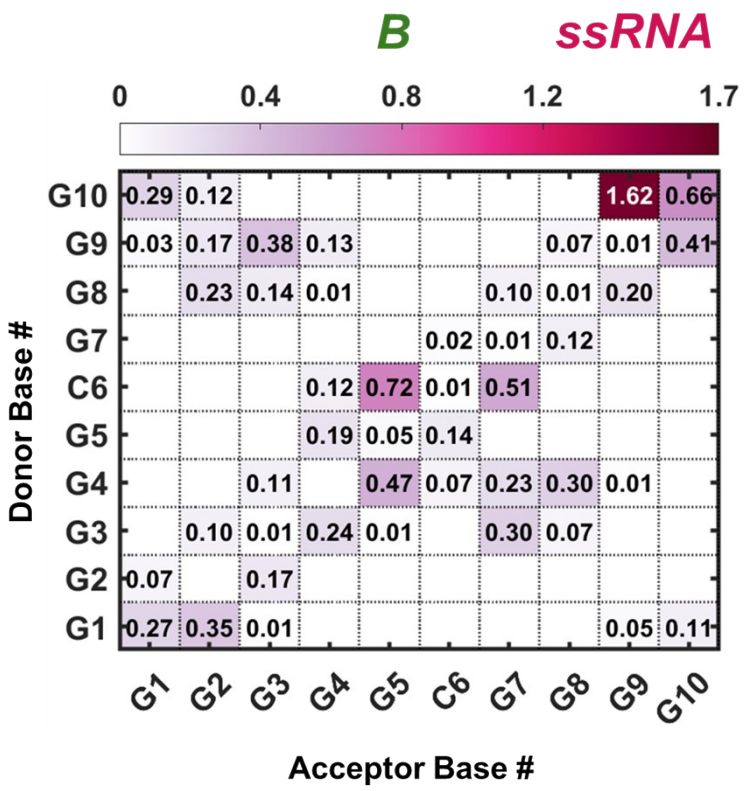

Figure S6-(iii): Hydrogen-bond (H-bond) heatmaps in time window – B, ranging from 85 to 150 ns, where overall ΔP_{dis} is low. The large off-diagonal numbers show hydrogen bonding between non-adjacent bases in comparison to the time windows in A and C, which are shown in Figure S6 (ii) and (iv).

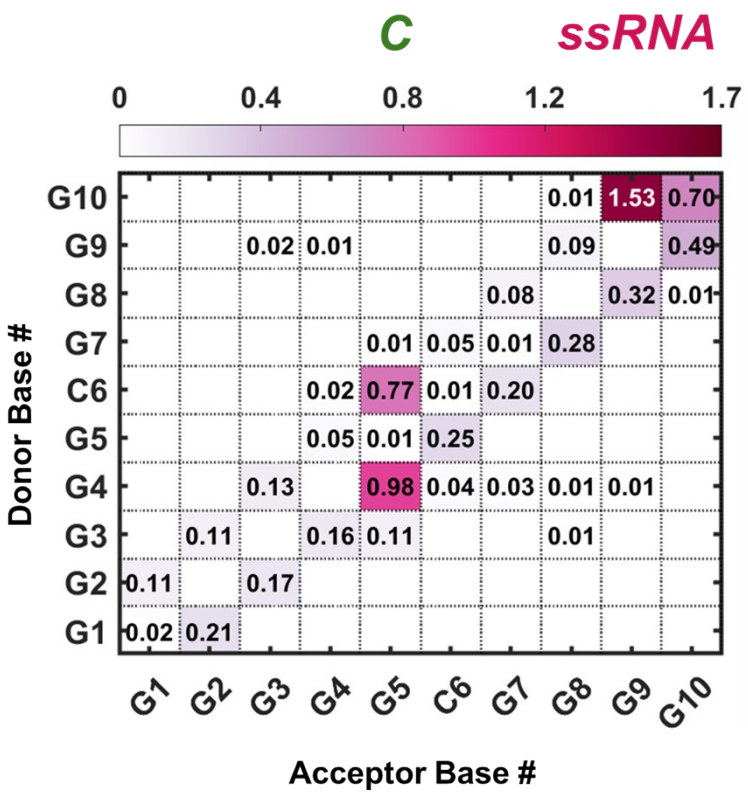

Figure S6-(iv): Hydrogen-bond (H-bond) heatmaps in time window – C, ranging from 150 to 200 ns, where overall ΔP_{dis} is high.

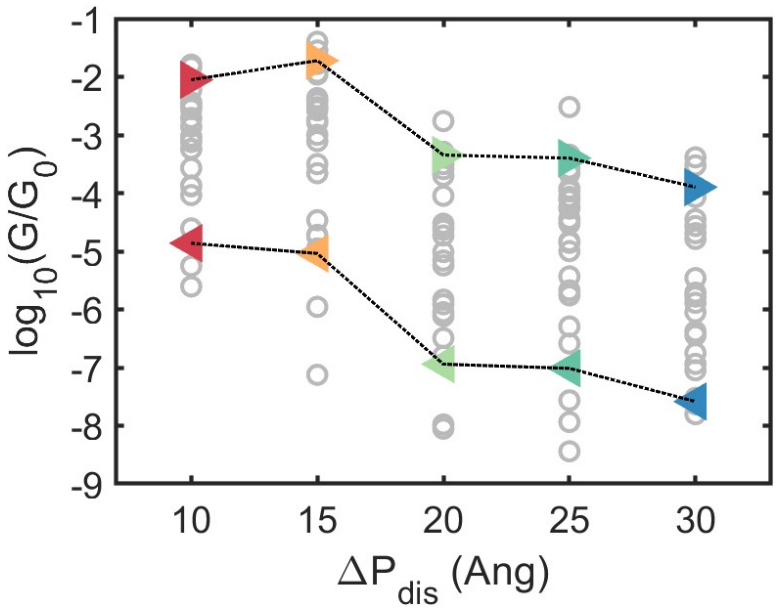

Figure S7: $^{\Delta P_{dis}}$ category-wise conductance spectrum (see the grey circles). The 10th and 90th percentiles (represented by lower and upper dotted envelopes, respectively) of conductance values for each $^{\Delta P_{dis}}$ category are also shown. The average conductance decreases from folded ($^{\Delta P_{dis} = 10, 15\ \text{Å}}$) to unfolded ($^{\Delta P_{dis} = 25, 30\ \text{Å}}$) states. Additionally, the conductance spread increases for larger $^{\Delta P_{dis}}$ values.

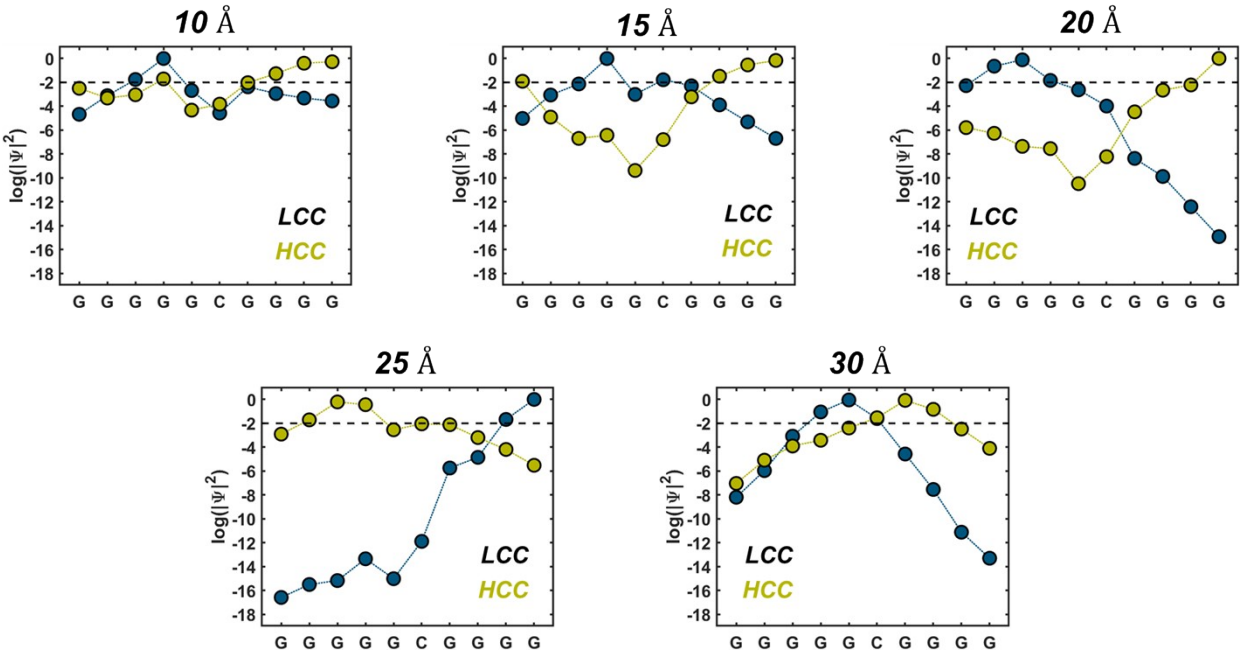

Figure S8: Probability of finding an electron at HOMO energy level for LCCs and HCCs for all $^{\Delta P_{dis}}$ categories.

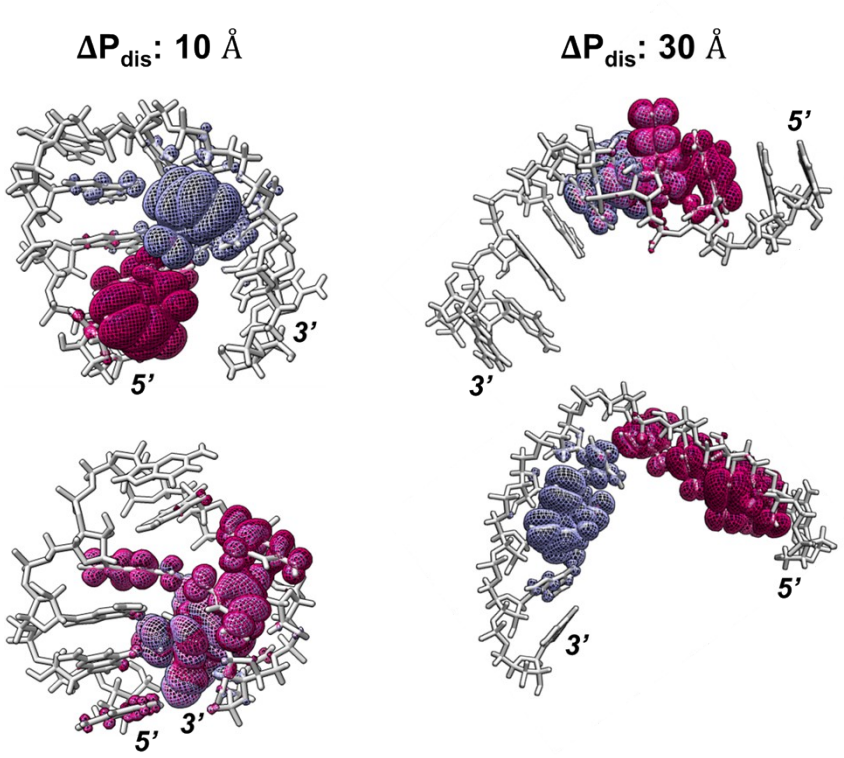

Figure S9: Orbital maps at HOMO and HOMO-1 energy levels for LCCs (top row) and HCCs (bottom row) for ΔP_{dis} = 10 and 30 Å. Higher delocalization can be observed at both energy levels for HCCs, compared to LCCs.

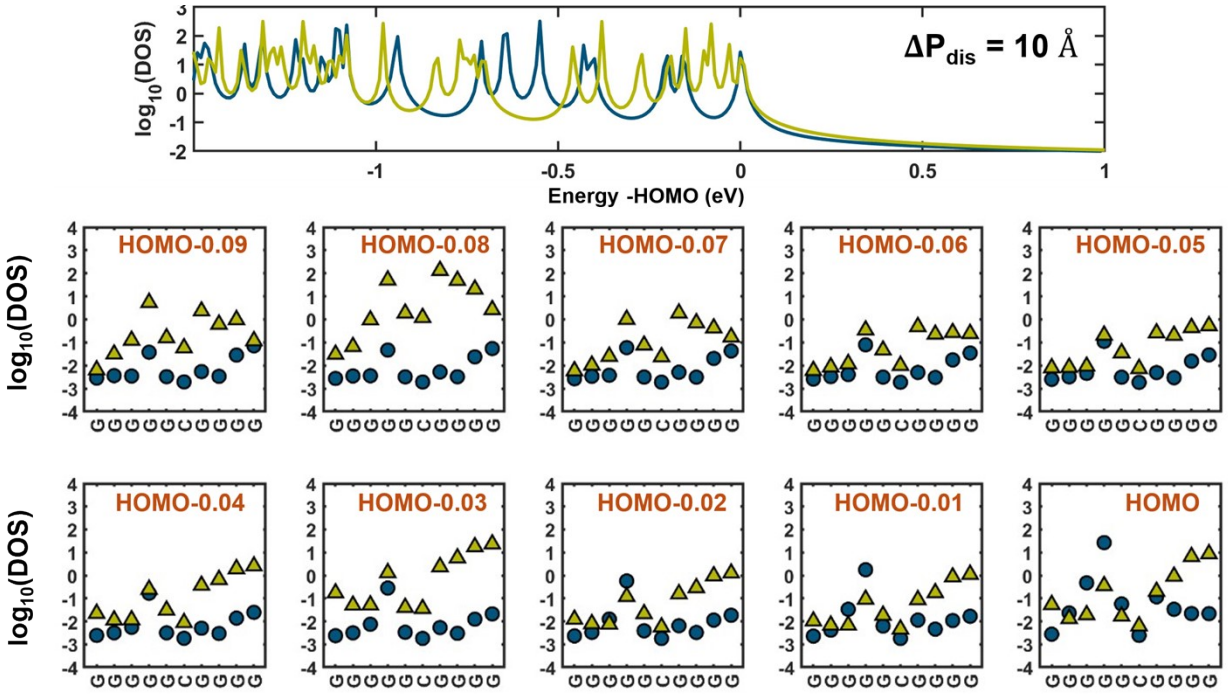

Figure S10: (Top row) Total DOS for $^{\Delta P_{dis}}$ = 10 Å. (Middle and bottom rows) Partial DOS at each base (sum of local density of states over all atoms at each base) between HOMO – (0.09 eV) and HOMO. In all subplots, HCC and LCC are represented in greenish-yellow and dark teal colors, respectively.

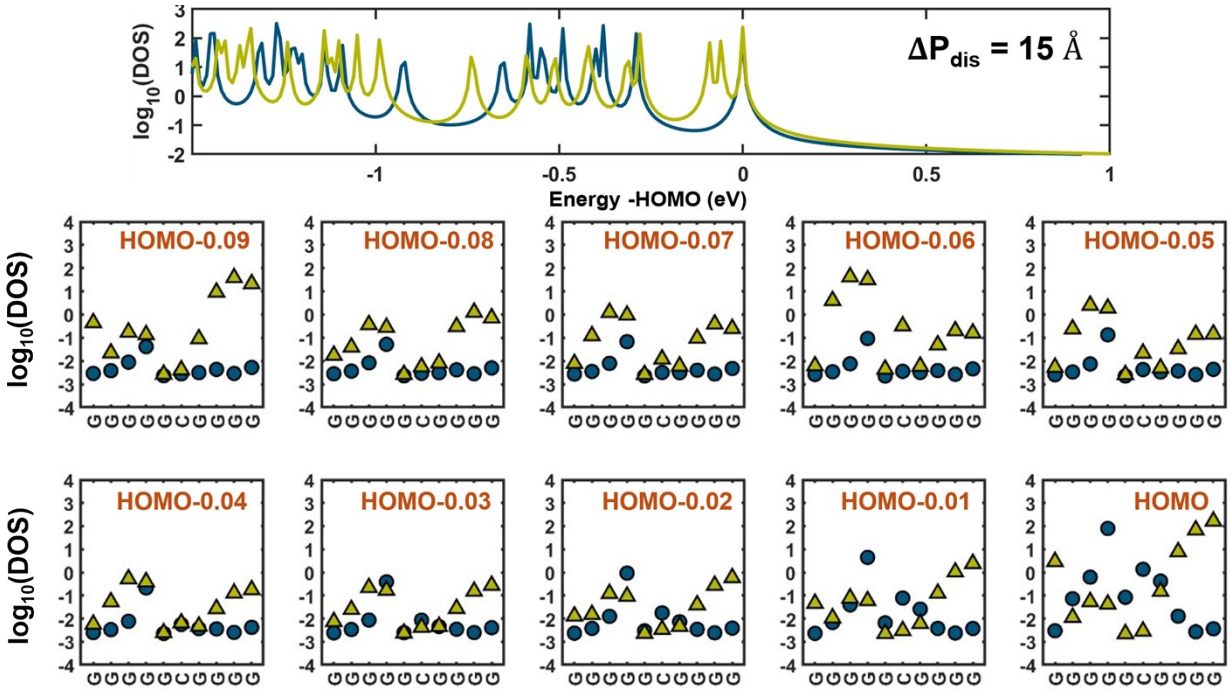

Figure S11: (Top row) Total DOS for $^{\Delta P_{dis}}$ = 15 Å. (Middle and bottom rows) Partial DOS at each base (sum of local density of states over all atoms at each base) between HOMO – (0.09 eV) and HOMO. In all subplots, HCC and LCC are represented in greenish-yellow and dark teal colors, respectively.

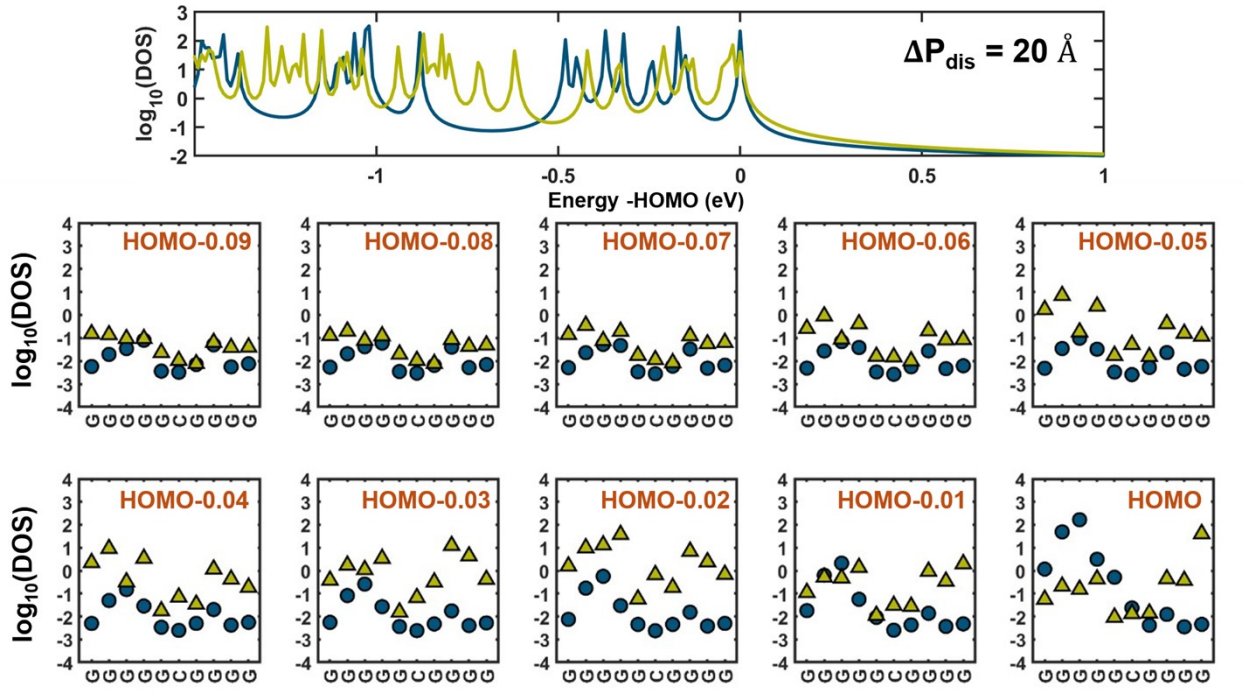

Figure S12: (Top row) Total DOS for $^{\Delta P}{}_{dis} = 20$ Å. (Middle and bottom rows) Partial DOS at each base (sum of local density of states over all atoms at each base) between HOMO – (0.09 eV) and HOMO. In all subplots, HCC and LCC are represented in greenish-yellow and dark teal colors, respectively.

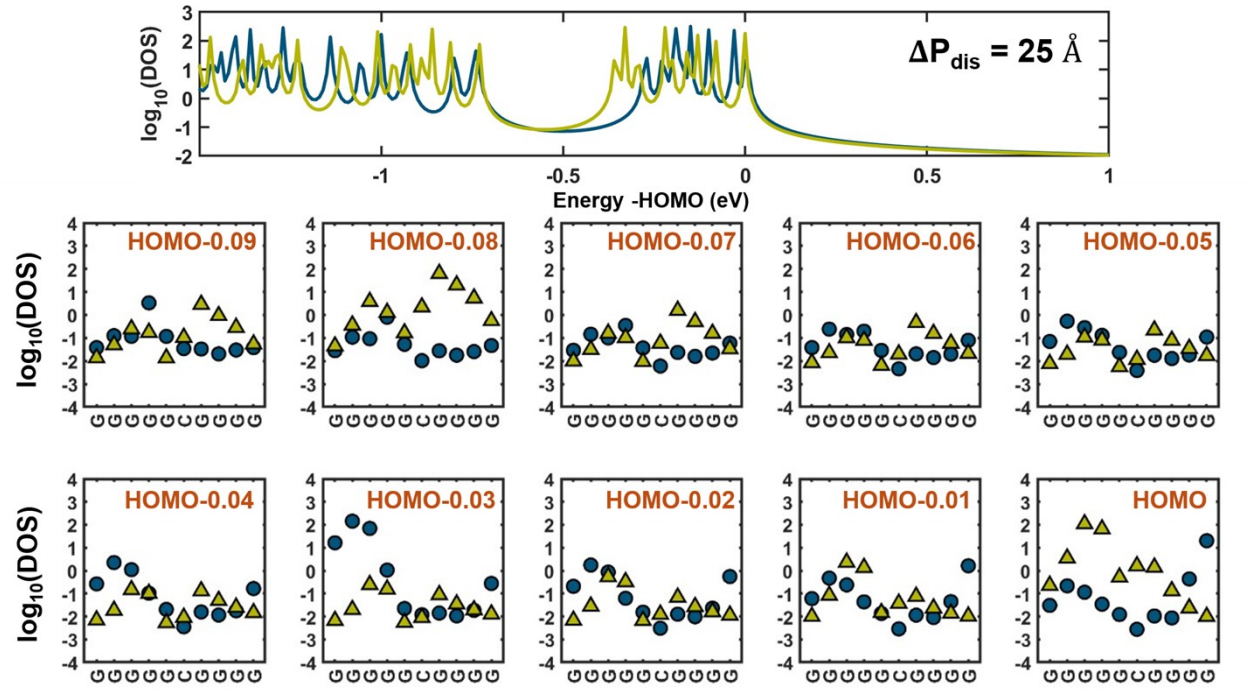

Figure S13: (Top row) Total DOS for $^{\Delta P_{dis}} = 25$ Å. (Middle and bottom rows) Partial DOS at each base (sum of local density of states over all atoms at each base) between HOMO – (0.09 eV) and HOMO. In all subplots, HCC and LCC are represented in greenish-yellow and dark teal colors, respectively.

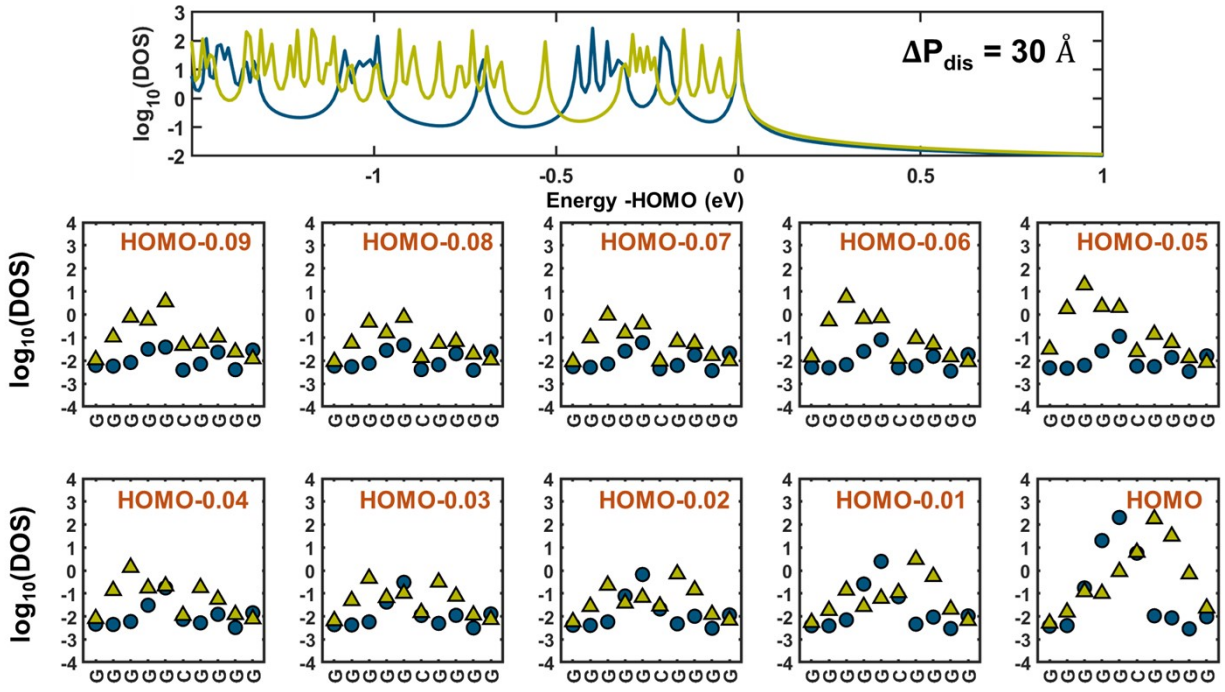

Figure S14: (Top row) Total DOS for $^{\Delta P_{dis}} = 30$ Å. (Middle and bottom rows) Partial DOS at each base (sum of local density of states over all atoms at each base) between HOMO – (0.09 eV) and HOMO. In all subplots, HCC and LCC are represented in greenish-yellow and dark teal colors, respectively.

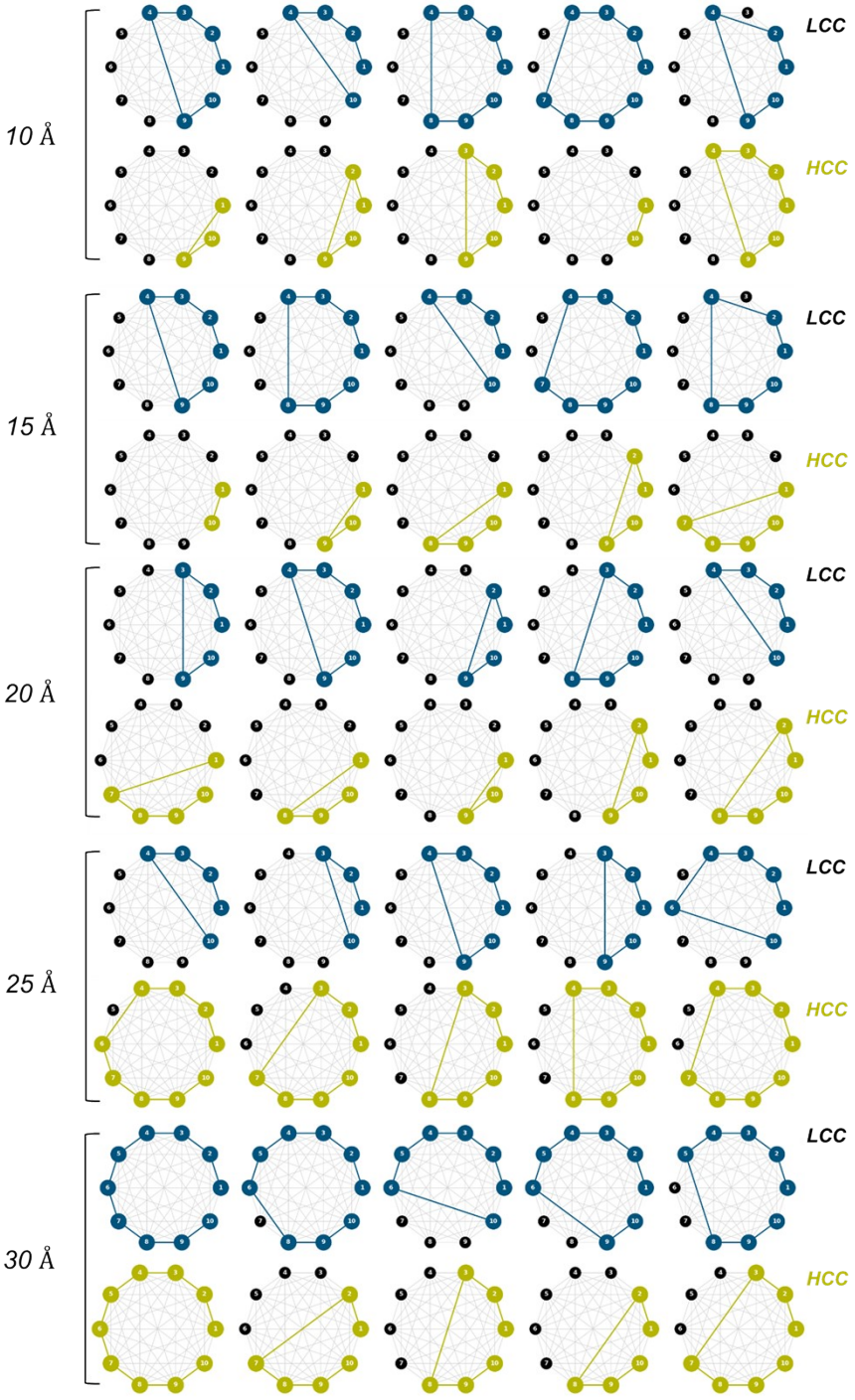

Figure S15: Top five probable paths for high conductance and low conductance conformations (HCC, LCC), $\Delta P_{dis} =$ 10, 15, 20, 25, and 30 Å.

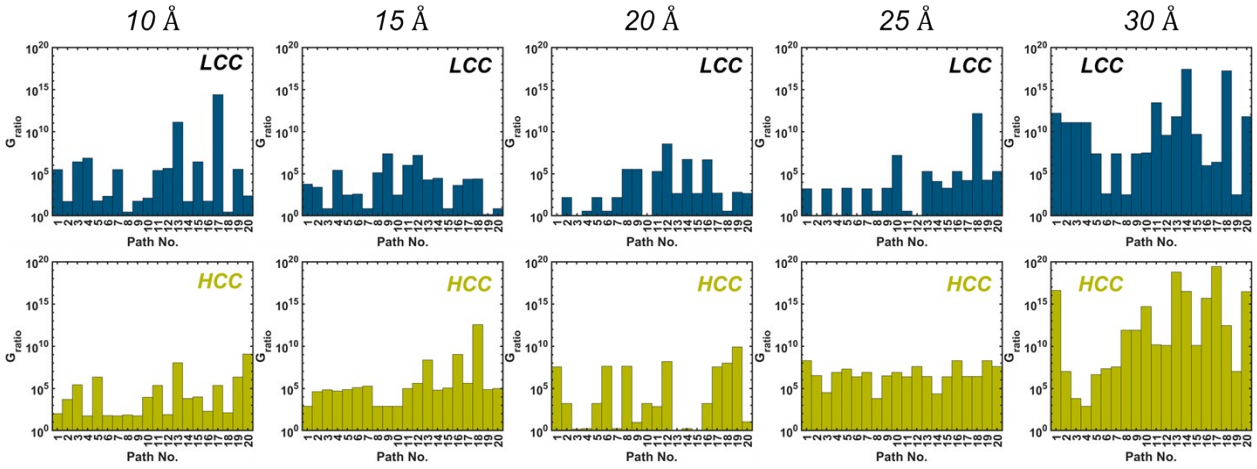

Figure S16: Ratio of conductance ($^{G_{pristine}}/_{G_{modified}}$) for each conformation when the hopping between nodes in a pathway is set to zero in the system Hamiltonian ($^{G_{modified}}$) to that computed with the pristine, unmodified Hamiltonian ($^{G_{pristine}}$). The top 20 paths have been shown.

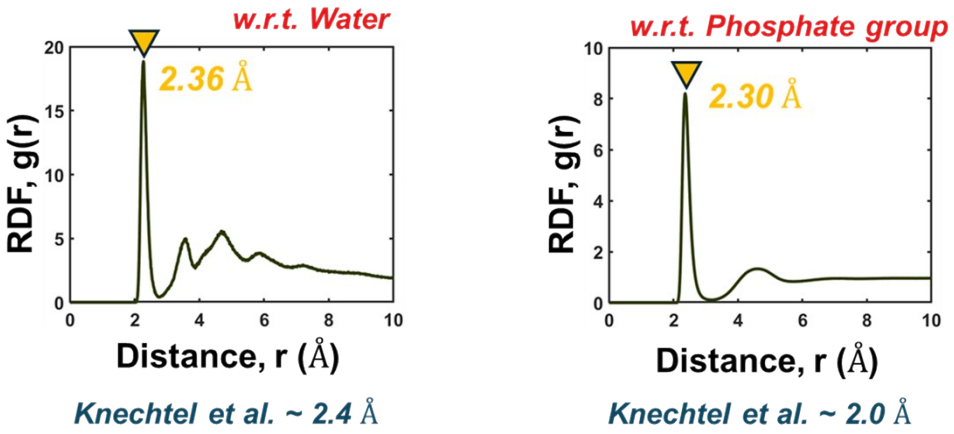

Figure S17: Comparison of radial distribution function (RDF) for sodium ions (Na+) with respect to (*left*) water (hydration shell) and (*right*) phosphate group with Knechtel et al.

Table S1: dsRNA Conductance data

Cluster No.	Conductance (G_0)
1	2.6606×10^{-4}
2	2.3602×10^{-4}
3	4.4622×10^{-5}
4	2.4000×10^{-3}
5	1.5267×10^{-4}

Table S2: Comparison of single-molecule conductances

Molecule	Sequence	Conductance ( )	Reference
dsRNA	$C_3(GC)_3C_2$	1.63 ± 0	1
DNA:RNA	$C_3(GC)_3C_2$	1.72 ± 0	
DNA:RNA	$C_3(GC)_3C_2$ [*A-form*] $C_3(GC)_3C_2$ [*Z-form*]	0.94 ± 0	2
ssRNA	CUC_2A	3.60 ± 0	3
ssRNA	CUC_2A_2CAUC	2.90 ± 0	
ssRNA	G_5CG_4	1.70 ± 5	This work
dsRNA	G_5CG_4	0.62 ± 0	

1. Chandra, S. *et al.* Single-molecule conductance of double-stranded RNA oligonucleotides. *Nanoscale* **14**, 2572–2577 (2022).
2. M. R. Aguilar, J. Jover, E. Ruiz, A. C. Aragonès, J. M. Artés Vivancos, Single-Molecule Electrical Conductance in Z-form DNA:RNA. Small 2025, 21, 2408459. https://10.1002/smll.202408459
3. Chandra, S. *et al.* Charge transport in individual short base stacked single-stranded RNA molecules. *Sci Rep* **13**, 19858 (2023).

PDB Files:

Coordinates of all the ssRNA and dsRNA structures considered in this work can be found here: https://github.com/AppyUW/ssRNA-Nanoscale-Horizon-2025.git